AGU PUBLICATIONS

Geophysical Research Letters

RESEARCH LETTER

10.1002/2014GL059997

Key Points:
- The PMM plays an important role in CP ENSO events
- Thermocline variations play an important role in EP ENSO events
- Defined CP and EP norms provide a tool for examining CP and EP ENSO events

Supporting Information:
- Readme
- Figure S1
- Figure S2
- Figure S3
- Text S1

Correspondence to:
D. J. Vimont,
dvimont@wisc.edu

Citation:
Vimont, D. J., M. A. Alexander, and M. Newman (2014), Optimal growth of Central and East Pacific ENSO events, *Geophys. Res. Lett.*, *41*, 4027–4034, doi:10.1002/2014GL059997.

Received 25 MAR 2014
Accepted 19 MAY 2014
Accepted article online 23 MAY 2014
Published online 11 JUN 2014

Optimal growth of Central and East Pacific ENSO events

Daniel J. Vimont[1,2], Michael A. Alexander[3], and Matthew Newman[3,4]

[1] Atmospheric and Oceanic Sciences Department, University of Wisconsin-Madison, Madison, Wisconsin, USA, [2] Nelson Institute Center for Climatic Research, University of Wisconsin-Madison, Madison, Wisconsin, USA, [3] Physical Sciences Division, Earth System Research Laboratory, NOAA, Boulder, Colorado, USA, [4] CIRES, University of Colorado Boulder, Boulder, Colorado, USA

Abstract Central Pacific (CP)-type and Eastern Pacific (EP)-type El Niño and the Southern Oscillation (ENSO) events are investigated using linear inverse modeling. Optimal initial conditions and growth rates for CP or EP ENSO events are identified explicitly using a CP or EP ENSO norm. The dominant difference in initial conditions that lead to CP and EP ENSO events is the role of the second empirical orthogonal function of tropical sea surface temperature, which represents the Pacific Meridional Mode (PMM). Optimal initial conditions for CP-type ENSO events include warm SST anomalies in the central subtropical Pacific (a characteristic of the PMM) while optimal initial conditions for EP-type ENSO events are focused in the eastern equatorial Pacific and Southern Hemisphere subtropics along about 25°S. Thermocline anomalies differ in initial structures and in their influence on SST for CP and EP events. Results point to different roles of the PMM and thermocline variations in the evolution of CP and EP ENSO events.

1. Introduction

Variations associated with the El Niño and the Southern Oscillation (ENSO) phenomenon are the dominant source of interannual climate variability around the globe [*Wallace et al.*, 1998]. The "canonical" warm ENSO event (El Niño) includes warming of sea surface temperature (SST) in the central and eastern equatorial Pacific and a reduction in east-to-west sea level pressure gradient (the Southern Oscillation) [*Walker*, 1924]. Recent research has highlighted differences between various ENSO events, with a principal characteristic being the longitudinal location of the maximum equatorial warming [*Trenberth and Stepaniak*, 2001; *Larkin and Harrison*, 2005; *Ashok et al.*, 2007; *Kao and Yu*, 2009; *Kug et al.*, 2009]. Specifically, two different types of ENSO events have been identified with maximum warming in the eastern equatorial Pacific (EP events; also referred to as canonical, conventional, or cold tongue events) or maximum warming in the central equatorial Pacific (CP events; also referred to as ENSO Modoki or warm pool events).

Two significant differences between the evolution of EP and CP ENSO events include an important role for northern subtropical SST anomalies in the generation of CP events but not in EP events [*Yu et al.*, 2010] and a propagation of thermocline anomalies along the equatorial Pacific during EP events that is not as evident in CP events (*Yu et al.* [2011], and inferred through sea level variations in *Kug et al.* [2009]). The evolution of northern subtropical SST anomalies appears to follow the seasonal footprinting mechanism [*Vimont et al.*, 2001, 2003a, 2003b], including precursor sea level pressure variations associated with the atmospheric North Pacific Oscillation [*Yu and Kim*, 2011]. *Chiang and Vimont* [2004] relate these northern subtropical SST anomalies to the Pacific Meridional Mode (PMM), and *Chang et al.* [2007] show that the seasonal footprinting mechanism's influence on ENSO operates through the PMM. Several studies, including *Ashok et al.* [2007], indicate that CP and EP ENSO are two fundamentally different phenomena, while others, e.g., *Yu et al.* [2010] and *Takahashi et al.* [2011], indicate that they are different manifestations of the same nonlinear evolution of ENSO.

Newman et al. [2011a] successfully simulate characteristics of CP and EP ENSO events using linear inverse modeling. Their analysis finds the leading two "L2 Norm" optimal structures identified by optimizing growth of domain mean square amplitude SST anomalies, which evolve into ENSO patterns with structures similar to CP or EP ENSO events, respectively. However, maximizing overall SST anomaly amplification throughout the tropics may combine different processes and/or phenomena and does not explicitly target growth rates of CP or EP ENSO events or initial structures that may lead to CP and EP ENSO events. In this analysis, we explicitly investigate CP or EP ENSO events separately using a CP or EP norm to evaluate growth and optimal

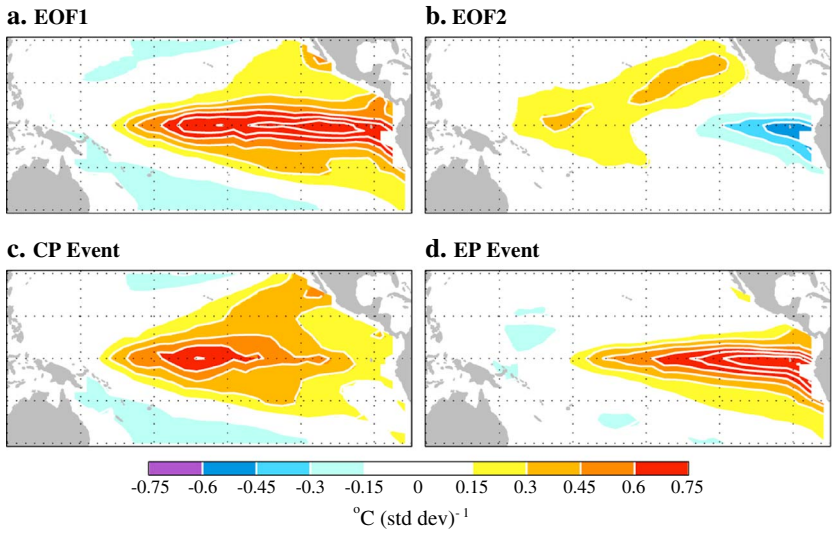

Figure 1. SST spatial structure for (a) EOF1, (b) EOF2, (c) CP ENSO event, and (d) EP ENSO event (see text for definitions). Units are in °C (standard deviation)$^{-1}$.

initial conditions. Data and methodology (section 2), results (section 3), and a discussion of the results (section 4) are presented.

2. Central and East Pacific ENSO Events

We first perform empirical orthogonal function/principal component (EOF/PC) analysis on tropical Pacific SST and thermocline depth (defined as depth of the 20°C isotherm; Z20). SST data were taken from the Hadley Centre Global Sea Ice and Sea Surface Temperature (HadISST) product [*Rayner et al.*, 2003] over the region 120°E–75°W, 30°S–30°N from 1958 to 2008. Thermocline depth was calculated from the Simple Ocean Data Assimilation product, version 2.1.6 [*Carton and Giese*, 2008], and was defined over the region 120°E–75°W, 20°S–20°N from 1958 to 2008. All data were averaged over 2° latitude by 5° longitude boxes and smoothed temporally using a 3 month running mean. EOF analysis was applied separately to SST and Z20. The spatial structures of SST EOF1 and SST EOF2 (multiplied by the square root of their respective eigenvalues so that units are in °C (standard deviation)$^{-1}$) are shown in Figures 1a and 1b. The leading EOF (Figure 1a) depicts a standard ENSO event while the second EOF depicts a structure that strongly resembles the Pacific Meridional Mode [*Chiang and Vimont*, 2004]; the correlation between the second PC and the PMM SST index ($r = 0.90$) confirms the relationship between EOF2 and the PMM. The use of EOF1 to depict a "standard" ENSO event is justified below.

Takahashi et al. [2011] use a linear combination of the first two principal components of tropical Pacific SST to define time series of Central Pacific (CP) and Eastern Pacific (EP) ENSO events. We choose to use the same definition in this study so that the CP and EP time series are linear combinations of the first two principal components of SST and as such are completely contained within the SST state vector that we use for linear inverse modeling (described below). We have repeated much of the analysis by defining CP and EP events according to the Niño 4 and Niño 1+2 indices and have found qualitatively similar results. This is not particularly surprising given the similarity between these indices and the CP and EP indices (see *Takahashi et al.* [2011]). The CP and EP time series are defined as

$$\mathrm{CP} = \left(\mathrm{PC1}/\sqrt{\lambda_1} + \mathrm{PC2}/\sqrt{\lambda_2}\right)/\sqrt{2} \tag{1}$$

$$\mathrm{EP} = \left(\mathrm{PC1}/\sqrt{\lambda_1} - \mathrm{PC2}/\sqrt{\lambda_2}\right)/\sqrt{2}. \tag{2}$$

Accordingly, the spatial structure of a CP or EP ENSO event is defined using the same linear combination of the EOFs (multiplied by the square roots of their respective eigenvalues) and is shown in Figures 1c and 1d (bottom). The resulting structures reproduce the results of *Takahashi et al.* [2011] including temporal variations (not shown).

3. Optimal Growth of CP and EP ENSO Events

Linear inverse modeling (LIM) is used to investigate optimal initial conditions that grow into CP or EP ENSO events. We provide a very brief description of our analysis method here; details of the derivation of the LIM and optimal initial structures can be found in *Penland and Sardeshmukh* [1995], *Tziperman et al.* [2008], and *Vimont* [2012]. In short, LIM operates under the assumption that the system trajectory can be described by the linear model

$$\frac{d\mathbf{x}}{dt} = \mathrm{L}\mathbf{x} + \xi. \tag{3}$$

We seek structures that experience growth from an initial condition $x(0)$ to a final condition $x(\tau)$ over a time period τ. This is obtained via solving the homogeneous version of (3)

$$\mathbf{x}(\tau) = \exp(\mathrm{L}\tau)\mathbf{x}(0) \equiv \mathrm{G}_\tau\mathbf{x}(0) \tag{4}$$

Growth, $\mu(\tau)$, is defined as the norm of the final condition $\mathbf{x}(\tau)$ divided by the norm of the initial condition $\mathbf{x}(0)$

$$\mu(\tau) = \frac{||\mathbf{x}(\tau)||_N^2}{||\mathbf{x}(0)||_M^2} \equiv \frac{\mathbf{x}(\tau)^T\mathrm{N}\mathbf{x}(\tau)}{\mathbf{x}(0)^T\mathrm{M}\mathbf{x}(0)} = \frac{\mathbf{x}(0)^T\mathrm{G}_\tau^T\mathrm{N}\mathrm{G}_\tau\mathbf{x}(0)}{\mathbf{x}(0)^T\mathrm{M}\mathbf{x}(0)} \tag{5}$$

where N and M are the final and initial norms, respectively. In the case of the Euclidean (L2) norm, N = M = I, the identity matrix. For the analysis herein, we wish to maximize growth of particular structures, specifically the CP and EP ENSO events without constraint on the initial conditions. So we use the L2 norm for the initial norm and construct CP and EP final norms.

The state vector $\mathbf{x}$ here is defined following the methodology of *Newman et al.* [2011b] using both SST and Z20

$$\mathbf{x} = \begin{bmatrix} \mathbf{z}_{SST} \\ \mathbf{z}_{Z20} \end{bmatrix} \tag{6}$$

where $\mathbf{z}_{SST}$ is the leading nine nonnormalized SST PCs (84.5% variance explained) and $\mathbf{z}_{Z20}$ is the leading three Z20 PCs (47% variance explained) resulting from the EOF/PC analysis described above. Note that there are fewer PCs used relative to *Newman et al.* [2011b] because here we use only the Pacific domain. Also, we repeated the analysis adding the leading two PCs of 10 m zonal wind over the Pacific and results did not change substantially (see supporting information). For simplicity, we use only the SST and Z20 PCs. With the above state vector, the *Takahashi et al.* [2011] definition of the CP and EP events facilitates construction and interpretation of a final norm. The analysis was repeated (not shown) using a Niño 4 or Niño 1+2 norm (defined via the method discussed in *Vimont* [2012]), and results were qualitatively similar. Note that a row vector defining the CP and EP coordinate directions is defined as follows:

$$\mathbf{n}_{\mathrm{CP}} = \left\{1/\sqrt{2\lambda_1}, 1/\sqrt{2\lambda_2}, 0, 0, \ldots\right\} \tag{7}$$

$$\mathbf{n}_{\mathrm{EP}} = \left\{1/\sqrt{2\lambda_1}, -1/\sqrt{2\lambda_2}, 0, 0, \ldots\right\}. \tag{8}$$

As such, the associated CP and EP final norms are defined as

$$\mathrm{N}_{\mathrm{CP}} = \mathbf{n}_{\mathrm{CP}}^T\mathbf{n}_{\mathrm{CP}} + \epsilon\mathrm{I} \tag{9}$$

$$\mathrm{N}_{\mathrm{EP}} = \mathbf{n}_{\mathrm{EP}}^T\mathbf{n}_{\mathrm{EP}} + \epsilon\mathrm{I} \tag{10}$$

where a small scalar multiple of the identity matrix is added for numerical stability [*Tziperman et al.*, 2008]. Note that with the definition of N in (9) and (10), the numerator in (5) can be rewritten as $[\mathbf{n}\mathrm{G}_\tau\mathbf{x}(0)]^T[\mathbf{n}\mathrm{G}_\tau\mathbf{x}(0)]$. This is simply the squared amplitude of the projection of a CP or EP ENSO event ($\mathbf{n}$) onto the final state $[\mathrm{G}_\tau\mathbf{x}(0)]$ and shows that the use of a CP or EP final norm in (5) simply indicates growth in the direction of a CP or EP ENSO event.

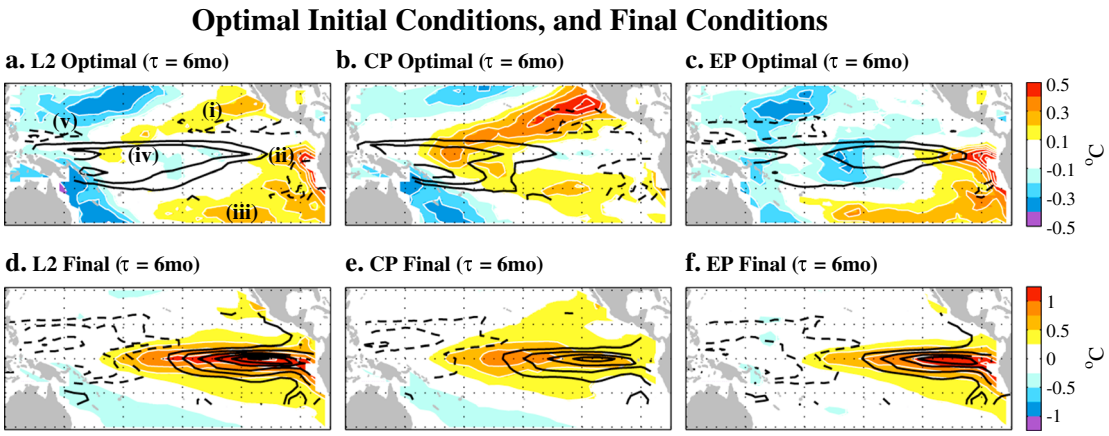

Figure 2. (a–c) τ = 6 month optimal initial and (d–f) associated final structures calculated under the L2 (Figures 2a and 2d), CP (Figures 2b and 2e), and EP (Figures 2c and 2f) norms. SST is shaded (contour 0.1°C in Figures 2a–2c and contour 0.25°C in Figures 2d–2f)), and Z20 variations are contoured in black (contour 1.6m in Figures 2a–2c) and contour 4 m in Figures 2d–2f); solid contours denote positive values, dashed contours denote negative values, and the zero contour has been omitted). Note that the contour interval for the final condition is 2.5 times the contour interval for the optimals.

Optimal initial conditions ($\mathbf{p}$) that maximize growth toward a standard, CP, or EP ENSO event over a given lag τ can be calculated from the L2, CP, or EP final norm via solving the generalized eigenvalue problem [*Zanna and Tziperman*, 2005]

$$\mathrm{G}_\tau^T \mathrm{N}_* \mathrm{G}_\tau \mathbf{p}_* - \mu_*(\tau)\mathbf{p}_* = \mathbf{0} \tag{11}$$

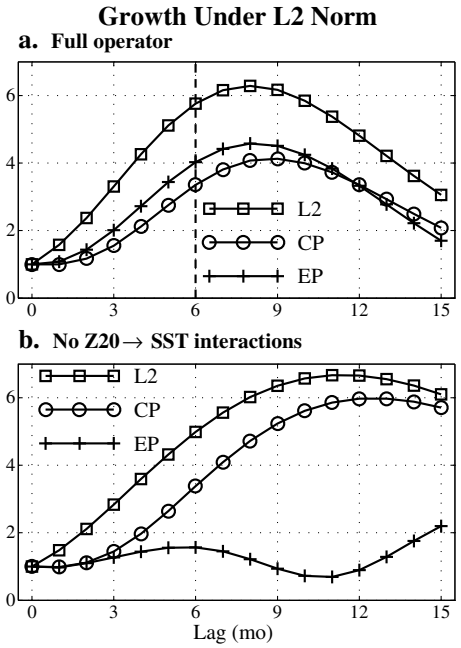

Figure 3. Growth rates under the L2 norm (i.e., as calculated by using the identity norm for N and M in (5)). Optimal initial conditions are still calculated by solving (11) using the L2 (squares), CP (circles), and EP (pluses) final norm (see text). (a) Optimal initial conditions and growth rates are calculated from the full dynamical operator. (b) Optimal initial conditions and growth rates are calculated from a dynamical operator in which Z20 → SST interactions have been suppressed (see text).

where the subscript $*$ on N indicates a specified final norm (L2, CP, or EP) and the subscript $*$ on $\mathbf{p}$ or μ indicates that the quantity is calculated from that specified final norm. The optimal initial structure $\mathbf{p}_{L2}$, $\mathbf{p}_{CP}$ or $\mathbf{p}_{EP}$ is referred to as the L2, CP, or EP optimal, respectively, and is plotted for a lag of 6 months in Figure 2 (top). We note that the 6 month lagged correlations between the time evolution of the L2, CP, and EP 6 month optimal initial conditions and PC1, CPC, and EPC are 0.64, 0.89, and 0.65, respectively, indicating that the LIM is appropriate for investigating the variability in question (see supporting information).

The L2 optimal in Figure 2 bears a strong resemblance to previous research: *Penland and Sardeshmukh* [1995] show a very similar structure in SST using an SST-only LIM, and *Newman et al.* [2011a] find a similar SST and Z20 structure using their SST/Z20/wind stress LIM. The L2 optimal is also nearly identical to an optimal calculated from an EOF1 final norm $\left(\text{i.e., } \mathbf{n}_{EOF1} = \left\{1/\sqrt{\lambda_1}, 0, 0, \ldots\right\}\right)$ which justifies the use of EOF1 to describe a standard ENSO event. Key features of the L2 optimal that we will discuss are labeled in Figure 2a, and include (i) positive northern subtropical SST anomalies in a diagonal band extending from about 0°, 180° northeastward to about 30°N, 120°W (this feature is also prominent in EOF2), (ii) positive equatorial SST anomalies east of about 130°W (prominent in the opposite polarity of EOF2), (iii) positive southern subtropical SST anomalies in a zonal band along about 25°S from the dateline to the eastern edge

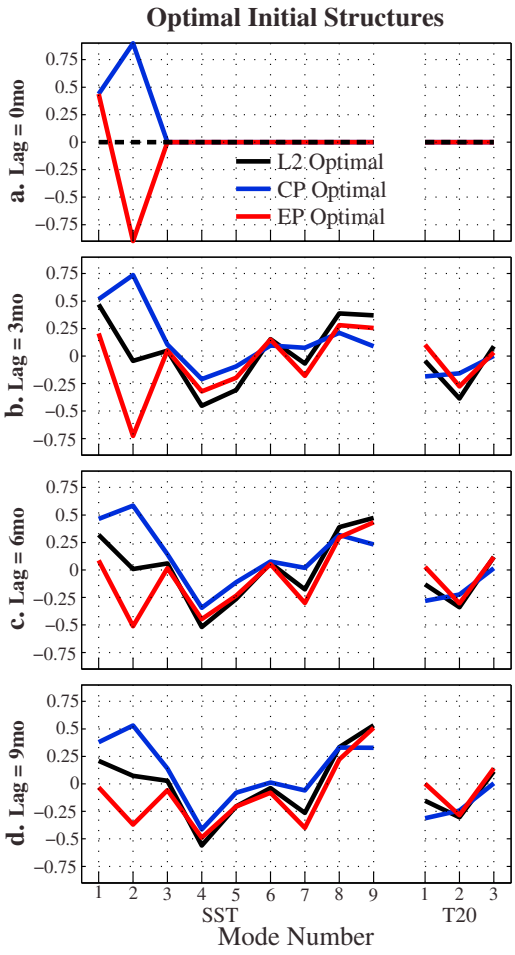

Figure 4. L2 (black), CP (blue), and EP (red) optimal initial conditions in their original EOF/PC space as a function of lag. Lags shown are (a) 0 months, (b) 3 months, (c) 6 months, and (d) 9 months. Note that the L2 optimal is not physically meaningful for lag 0.

of the basin, (iv) positive thermocline depth anomalies along the equator, and (v) weak negative thermocline depth anomalies at about 7°N in the western tropical Pacific. The L2 optimal generates a standard ENSO event as a final condition over 6 months (Figure 2d), which is confirmed by the state vector for the final condition, which is dominated by EOF1 (not shown) of SST and Z20.

Comparison between the structure of the L2 optimal and the CP or EP optimal illustrates important differences in the relative importance of SST anomalies and thermocline anomalies in the five regions highlighted in Figures 2a. The positive northern subtropical SST anomalies (feature(i)) are much more pronounced in the CP optimal (Figure 2b), consistent with the positive polarity of EOF2 in the CP norm. This highlights the importance of the PMM in influencing CP ENSO events. In contrast, the EP optimal (Figure 2c) shows very little signature of positive northern subtropical SST anomalies and instead emphasizes positive southern subtropical SST anomalies (feature (iii); this region is also highlighted in *Zhang et al.* [2013]) and positive equatorial SST anomalies (feature (ii)) consistent with the opposite polarity of EOF2 in the EP optimal. Thermocline depth anomalies in the equatorial Pacific (feature (iv)) also differ between the CP and EP events, with deeper thermocline anomalies confined to the central and western equatorial Pacific in the CP optimal, and deeper thermocline anomalies in the central equatorial Pacific for the EP optimal. In the far northwestern tropical Pacific (feature (v)) the CP optimal has positive thermocline depth anomalies (the contour is too large to show the positive anomalies) while the EP optimal has negative thermocline depth anomalies. The L2, CP, and EP optimals develop into a final condition over 6 months (Figure 2, second row) that resemble a canonical ENSO event (EOF1), a CP ENSO event, and an EP ENSO event, though the CP and EP final structures in Figures 2e and 2f do not differ spatially as much as the directly calculated CP or EP structure in Figures 1c and 1d, respectively.

Recall that optimal initial structures are calculated under a specified norm in order to maximize growth into a standard (L2), CP, or EP ENSO event. By construction, growth (from (5)) under a specific norm is only maximized when using the optimal initial condition that is calculated (by solving (11)) under that same norm. A common norm, then, is needed to compare growth from different initial conditions; the obvious choice for the common norm is the L2 norm. Figure 3 shows growth under the L2 norm (i.e., using the identity matrix for $\mathbf{N}$ and $\mathbf{M}$ in (5)) of the L2, CP, or EP optimal initial conditions (i.e., the optimal initial conditions that were calculated by solving (11) with a specified L2, CP, or EP final norm). Growth under the L2 norm (Figure 3a) maximizes at about 7–8 months for the L2 and EP optimals and about a month later for the CP optimal. The timing for maximum growth is consistent with a slightly longer duration of CP events than EP events. The L2 and EP optimals also experience more growth under the L2 norm than the CP optimal, though the difference between growth of the CP and EP optimal is small.

How important are thermocline variations in growth rates of the CP and EP ENSO events? The dynamical system matrix L can be split into four parts (as in *Newman et al.* [2011b]) that include influences among SST modes(the upper left 9×9 elements), among Z20 modes (the bottom right 3×3 elements), from SST modes

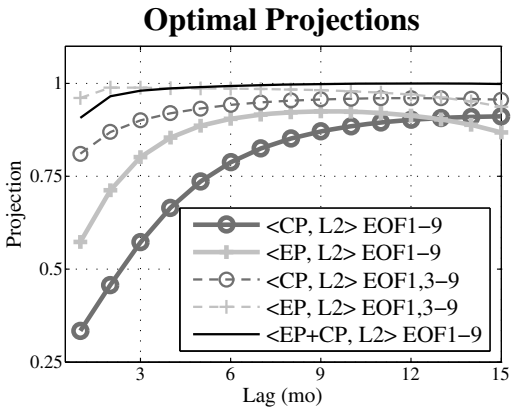

Figure 5. Projection of the CP (dark grey with circles) and EP (light grey with pluses) optimal initial structures onto the L2 optimal. Thick solid lines denote projections of the full optimal (modes 1–9); thin dashed lines denote projections using only modes 1 and 3–9. Thin solid black line denotes the projection of the average of the CP and EP optimal onto the L2 optimal.

to Z20 modes (the bottom left 3×9 elements), and from Z20 modes to SST modes (the top right 9×3 elements). By zeroing the upper right 9×3 elements, the effect of thermocline variations on SST is eliminated. When optimal structures and growth rates (under the L2 norm) are recalculated under this "Z20 → SST suppressed" dynamical system, the growth rates from the L2 and CP optimals are nearly identical for lags less than about 7 months, but growth from the EP optimal nearly vanishes (Figure 3b). This highlights the importance of thermocline variations in EP events in comparison with CP events [*Kug et al.*, 2009; *Yu et al.*, 2010; *Messié and Chavez*, 2013].

The different optimal structures in Figures 2a–2c highlight different contributions from EOF2 and are somewhat expected based on the way the CP or EP norms are constructed. To further examine the contribution of EOF2 to the CP and EP optimals, we plot the CP and EP optimals (in PC space) as a function of lag in Figure 4. At lag 0, calculation of the optimal yields the CP and EP norms themselves (solutions under the L2 norm for lag 0 are not physically meaningful) which are plotted in Figure 4a and which highlight the opposing role for EOF2 in a CP or EP ENSO event. The opposing role for EOF2 is maintained in the optimal structures at lags 3, 6, and 9 (Figures 4b, 4c, and 4d) while the higher order modes contribute nearly identically to the L2, CP, and EP optimals. We note that EOF1 also contributes significantly to the CP optimal initial condition for lags 3–9 months but not to EP initial conditions, perhaps reflecting a longer persistence of CP events. For each lag, the L2 optimal is nearly an average of the CP and EP optimals. Figure 4 shows that the role of EOF2 is the dominant difference between the three optimals.

To further quantify the similarities and differences between the optimals, the projection of the CP and EP optimal onto the L2 optimal is plotted in Figure 5. The CP optimal differs most from the L2 optimal, especially for small lead times under which the optimals are calculated. Both the CP and EP optimals are quite similar to the L2 optimal for large lags. The importance of EOF2 to the EP and CP optimal can be evaluated by removing EOF2 from the optimal pattern and recalculating the projection over modes 1 and 3–12. Projections without EOF2 are all larger than the projections that include EOF2 and differ substantially for lags shorter than about 6–9 months. These projections support the sense that EOF2 is the dominant contributor to differences between the optimals. Finally, the projection of the average of the EP and CP optimals onto the L2 optimal is very close to 1 for all lags, indicating that the standard ENSO optimal is nearly numerically equivalent to the average of the CP and EP optimals.

How can we interpret the optimal structures for standard, CP, and EP ENSO events? First, we note that the major differences between the optimal structures are the roles of SST EOF1 (the current state of ENSO) and of EOF2 (the PMM). The remaining modes contribute in nearly the same way to the development of a standard, CP, or EP ENSO event. Consider, then, conditions among SST modes 3–9 and Z20 modes 1–3 that would tend to cause the system to evolve into a positive ENSO event (El Niño). If SST EOF1 and the PMM are in positive phases, then the resulting El Niño event should have more CP characteristics. If the PMM is in a negative phase, then the resulting El Niño event should have more EP characteristics. Assuming linearity, the same argument would hold for the opposite polarity (negative ENSO or La Niña events) as well.

4. Summary and Discussion

Transient growth of Central Pacific (CP) and Eastern Pacific (EP) ENSO events is examined. The use of an EOF/PC-based definition of CP and EP ENSO events from *Takahashi et al.* [2011] facilitates construction of a norm under which transient growth is evaluated. Comparison of CP and EP optimals highlights the role of EOF2 (the Pacific Meridional Mode, PMM) in the origin of CP and EP ENSO events. In particular, optimal initial conditions for CP ENSO events include SST anomalies that are located in the northern subtropical Pacific in

a region where the PMM exhibits a maximum in variance, positive thermocline depth anomalies in the central and western equatorial Pacific, and positive thermocline depth anomalies in the northwestern tropical Pacific. Optimal initial conditions for EP ENSO events include positive SST anomalies in the eastern equatorial Pacific and southern subtropical Pacific (where the PMM does not exhibit a great deal of variance), positive thermocline depth anomalies in the central and eastern equatorial Pacific, and negative thermocline depth anomalies in the northwestern tropical Pacific. When the effect of Z20 on SST (Z20 → SST) is suppressed in the dynamical operator, growth rates for EP events nearly vanish, indicating a fundamentally different role for thermocline variations in EP events compared to CP events.

It is not clear whether the use of CP and EP norms identify fundamentally independent types of ENSO events. On one hand, it could be argued that the differing role of the SST EOF2 is built in to the calculation of the CP and EP optimals by virtue of the opposing sign of that EOF in the CP and EP norms. As such, one could argue that CP and EP definitions are artificial and simply force or eliminate (respectively) a role for the PMM in the development of ENSO events. Whether or not the system evolves into more of a CP or EP ENSO event then is simply determined by the particulars of the noise forcing for a given event [*Newman et al.*, 2011a]. On the other hand, that the L2 optimal is nearly exactly an average of the CP and EP optimal could also be interpreted as a statement that the standard ENSO event and ENSO optimal are simply a combination of the more physically meaningful CP and EP ENSO events. In this case, the different role of EOF2 may represent a fundamentally different dynamical pathway by which CP and EP ENSO events evolve (e.g., as suggested by *Aiken et al.* [2013]). The difference in growth rates in the Z20 → SST suppressed simulations support the interpretation that the events develop via different physical processes. In either case, any individual ENSO event is likely to be a combination of ENSO types [*Ray and Giese*, 2012]. The difference between the different types, however, motivates a more in-depth investigation of the role of EOF2, thermocline variations, and other features of the CP and EP optimals in the dynamics of the system.

How does this analysis add to our understanding of CP and EP ENSO events? This analysis highlights the different role of the PMM in exciting CP versus EP ENSO events. The PMM plays an important role in the Seasonal Footprinting Mechanism [*Vimont et al.*, 2001, 2003a, 2003b; *Chang et al.*, 2007], and its role in the various optimals is consistent with the findings that CP ENSO events are initiated via subtropical SST anomalies [*Yu et al.*, 2010]. Our results suggest that precursors to CP-type ENSO events may be well captured by the SST field (e.g., warm SST anomalies extending southwestward from Baja California), while precursors to EP-type ENSO events may be better captured by thermocline variations. Differences in growth rates when Z20 → SST interactions are suppressed also suggest that CP and EP ENSO events evolve via different physical mechanisms. Finally, the use of the CP and EP norms provides direction for further research into the dynamics of CP and EP ENSO events using LIM. In particular, the different norms provide a means for targeting various spatial structures (in both the ocean and atmosphere) and their relationship with both the dynamics and noise forcing of the system.

Acknowledgements
HadISST data were obtained online from the UK Met Office website at http://www.metoffice.gov.uk/hadobs/hadisst/. Simple Ocean Data Assimilation data were obtained online from the SODA/TAMU research group at http://soda.tamu.edu/. Support for D.J.V. was provided by the U.S. Department of Energy grant DE-SC0005301 and the Wisconsin Alumni Research Foundation. M.N. was supported from the NOAA/MAPP program.

The Editor thanks Laure Zanna and an anonymous reviewer for their assistance in evaluating this paper.

References

Aiken, C. M., A. Santoso, S. McGregor, and M. H. England (2013), The 1970's shift in ENSO dynamics: A linear inverse model perspective, *Geophys. Res. Lett.*, *40*, 1612–1617, doi:10.1002/grl.50264.

Ashok, K., S. K. Behera, S. A. Rao, H. Weng, and T. Yamagata (2007), El Niño Modoki and its possible teleconnection, *J. Geophys. Res.*, *112*, C11007, doi:10.1029/2006JC003798.

Carton, J. A., and B. S. Giese (2008), A reanalysis of ocean climate using Simple Ocean Data Assimilation (SODA), *Mon. Weather Rev.*, *136*, 2999–3017, doi:10.1175/2007MWR1978.1.

Chang, P., L. Zhang, R. Saravanan, D. J. Vimont, J. C. H. Chiang, L. Ji, H. Seidel, and M. K. Tippett (2007), Pacific meridional mode and El Niño-Southern oscillation, *Geophys. Res. Lett.*, *34*, L16608, doi:10.1029/2007GL030302.

Chiang, J., and D. Vimont (2004), Analogous Pacific and Atlantic Meridional Modes of tropical atmosphere-ocean variability, *J. Clim.*, *17*(21), 4143–4158.

Kao, H.-Y., and J.-Y. Yu (2009), Contrasting Eastern-Pacific and Central-Pacific types of ENSO, *J. Clim.*, *22*(3), 615–632, doi:10.1175/2008JCLI2309.1.

Kug, J.-S., F.-F. Jin, and S.-I. An (2009), Two types of El Niño Events: Cold tongue El Niño and warm pool El Niño, *J. Clim.*, *22*(6), 1499–1515, doi:10.1175/2008JCLI2624.1.

Larkin, N. K., and D. E. Harrison (2005), On the definition of El Niño and associated seasonal average U.S. weather anomalies, *Geophys. Res. Lett.*, *32*, L13705, doi:10.1029/2005GL022738.

Messié, M., and F. P. Chavez (2013), Physical-biological synchrony in the global ocean associated with recent variability in the central and western equatorial Pacific, *J. Geophys. Res. Oceans*, *118*, 3782–3794, doi:10.1002/jgrc.20278.

Newman, M., S.-I. Shin, and M. A. Alexander (2011a), Natural variation in ENSO flavors, *Geophys. Res. Lett.*, *38*, L14705, doi:10.1029/2011GL047658.

Newman, M., M. A. Alexander, and J. D. Scott (2011b), An empirical model of tropical ocean dynamics, *Clim. Dyn.*, *37*(9-10), 1823–1841, doi:10.1007/s00382-011-1034-0.

Penland, C., and P. Sardeshmukh (1995), The optimal growth of tropical sea surface temperature anomalies, *J. Clim.*, *8*, 1999–2024.
Ray, S., and B. S. Giese (2012), Historical changes in El Niño and La Niña characteristics in an ocean reanalysis, *J. Geophys. Res.*, *117*, C11007, doi:10.1029/2012JC008031.
Rayner, N. A., D. E. Parker, E. B. Horton, C. K. Folland, L. V. Alexander, D. P. Rowell, E. C. Kent, and A. Kaplan (2003), Global analyses of sea surface temperature, sea ice, and night marine air temperature since the late nineteenth century, *J. Geophys. Res.*, *108*(D14), 4407, doi:10.1029/2002JD002670.
Takahashi, K., A. Montecinos, K. Goubanova, and B. Dewitte (2011), ENSO regimes: Reinterpreting the canonical and Modoki El Niño, *Geophys. Res. Lett.*, *38*, L10704, doi:10.1029/2011GL047364.
Trenberth, K., and D. Stepaniak (2001), Indices of El Niño evolution, *J. Clim.*, *14*, 1697–1701.
Tziperman, E., L. Zanna, and C. Penland (2008), Nonnormal thermohaline circulation dynamics in a coupled ocean-atmosphere GCM, *J. Phys. Oceanogr.*, *38*, 588–604, doi:10.1175/2007JPO3769.1.
Vimont, D., D. Battisti, and A. Hirst (2001), Footprinting: A seasonal connection between the tropics and mid-latitudes, *Geophys. Res. Lett.*, *28*(20), 3923–3926.
Vimont, D., D. Battisti, and A. Hirst (2003a), The seasonal footprinting mechanism in the CSIRO general circulation models, *J. Clim.*, *16*, 2653–2667.
Vimont, D., J. Wallace, and D. Battisti (2003b), The seasonal footprinting mechanism in the Pacific: Implications for ENSO, *J. Clim.*, *16*, 2668–2675.
Vimont, D. J. (2012), Analysis of the Atlantic Meridional Mode using linear inverse modeling: Seasonality and regional influences, *J. Clim.*, *25*(4), 1194–1212, doi:10.1175/JCLI-D-11-00012.1.
Walker, G. T. (1924), Correlation in seasonal variations of weather, IX. A further study of world weather, *Mem. India Meteorol. Dept.*, *24*(9), 275–333.
Wallace, J. M., E. M. Rasmusson, T. P. Mitchell, V. E. Kousky, and E. S. Sarachik (1998), On the structure and evolution of ENSO-related climate variability in the tropical Pacific: Lessons from TOGA, *J. Geophys. Res.*, *103*(C7), 14,241–14,259, doi:10.1029/97JC02905.
Yu, J.-Y., and S. T. Kim (2011), Relationships between extratropical sea level pressure variations and the Central Pacific and Eastern Pacific Types of ENSO, *J. Clim.*, *24*(3), 708–720, doi:10.1175/2010JCLI3688.1.
Yu, J.-Y., H.-Y. Kao, and T. Lee (2010), Subtropics-related interannual sea surface temperature variability in the central equatorial Pacific, *J. Clim.*, *23*(11), 2869–2884, doi:10.1175/2010JCLI3171.1.
Yu, J.-Y., H.-Y. Kao, T. Lee, and S. T. Kim (2011), Subsurface ocean temperature indices for Central-Pacific and Eastern-Pacific types of El Niño and La Niña events, *Theor. Appl. Climatol.*, *103*(3-4), 337–344, doi:10.1007/s00704-010-0307-6.
Zanna, L., and E. Tziperman (2005), Nonnormal amplification of the thermohaline circulation, *J. Phys. Oceanogr.*, *35*, 1593–1605, doi:10.1175/JPO2777.1.
Zhang, H., A. Clement, and P. Di Nezio (2013), The South Pacific meridional mode: A mechanism for ENSO-like variability, *J. Clim.*, doi:10.1175/JCLI-D-13-00082.1.